

# On detection and estimation in atomic force microscopy at different scan speeds <sup>★</sup>

Peng Huang<sup>\*</sup> Sean B. Andersson<sup>\*\*</sup>

<sup>\*</sup> *Department of Mechanical Engineering, Boston University, Boston, MA 02215 USA (e-mail: huangp09@bu.edu).*

<sup>\*\*</sup> *Department of Mechanical Engineering and Division of Systems Engineering, Boston University, Boston, MA 02215 USA (e-mail: sanderss@bu.edu)*

---

## Abstract:

A typical user of an atomic force microscope (AFM) judges the quality of information in the scan of a sample by the images generated from either the height signal (in contact mode) or the height, amplitude, and phase signals (in intermittent contact mode). As the speed of the tip across the sample is increased, these signals become corrupted by the dynamics in the actuators and other elements in the system. The amplitude and phase signals are derived from the motion of the cantilever during the scan and there have been alternative schemes proposed, such as transient mode AFM, that derive several other signals from the cantilever motion. In this work we study the utility of the height, amplitude, and other derived signals at different tip speeds for both imaging and for detection. The results are demonstrated through experiments using a grating sample scanned on an Agilent 5500 AFM.

*Keywords:* atomic force microscopy, high speed imaging, tracking, Kalman observer.

---

## 1. INTRODUCTION

Since the invention of the Atomic Force Microscope (AFM) (Binnig and Quate, 1986) researchers have continually improved its temporal resolution. Approaches to high speed AFM include the use of advanced controllers (e.g. (Shan and Leang, 2012), (Wu and Zou, 2007)) and of novel mechanical designs (e.g. (Schaeffer et al., 1997), (Kenton et al., 2011)). State-of-the-art research systems can achieve video-rate imaging (e.g. (Braunsmann and Schaffer, 2010), (Kodera et al., 2010)), though with tradeoffs in available imaging modes or scanning size.

Despite these advances, most commercial instruments still rely on relatively simple proportional-integral-derivative type controllers for actuation in the vertical ( $z$ ) direction. This is due in no small part to concerns on the cost and complexity of high-speed instruments. As a result, the typical bandwidth of the  $z$ -direction is in the range of a few hundred Hz up to a few kHz, limiting the achievable frame rate when standard imaging is considered. There is still valuable information in the available signals, however, even when the frame rate (and thus the speed of the tip) is well beyond the typical “good” imaging rates.

There has been some effort in recent years on taking advantage of this information for imaging. One of the benefits of these approaches is that they are typically algorithmic in nature, making them simple to implement on existing

instruments to improve their temporal resolution. Further, then can also be used on high speed instruments for even faster imaging.

One example of such work is the transient-mode AFM (TM-AFM) in (Salapaka et al., 2005; Sahoo et al., 2005). Under this scheme the transients in the motion of the cantilever caused by interaction with the sample are monitored. TM-AFM yields a significantly faster imaging rate but at the cost of reduced information as the generated images in essence show only the edges of the sample.

A second example is the work of the authors (with others) on non-raster scanning. In (Chang et al., 2011), a Local Raster Scan (LRS) technique was developed that takes advantage of the idea of detection of events in the signals, as in the TM-AFM, and uses it to close a feedback loop that steers the tip to stay in the region of interest. An order of magnitude reduction in imaging time can be achieved but again at a cost; the technique is limited to string-like samples such as DNA, actin filaments, features edges, and similar. This idea of detection can in fact be carried even further. AFM has been used to observe dynamic processes, particularly in molecular biology (e.g., the motion of proteins (Viani et al., 2000) and of molecular motors (Kodera et al., 2010)). It is clear that in such scenarios, it is the *motion* not the *profile* of the sample that is often of interest. As a result, the measurements made by AFM can be completely separated from the notion of imaging and thus of the bandwidth limitations imposed by the vertical actuator. Early work along these lines by the authors included implementing and extending the TF-AFM method to address the direct *tracking* of objects using AFM (Huang and Andersson, 2012).

---

<sup>★</sup> This work was supported in part by NSF through grant CMMI-0845742 and by grants from the National Center for Research Resources (5R21RR025362-03) and the National Institute of General Medical Sciences (8 R21 GM103530-03) from the National Institutes of Health.

In this paper, we are interested primarily in applications in biology. We therefore consider only intermittent-contact (“tapping”) mode AFM. In this context, there are several signals typically available, including the height, amplitude and cantilever position. The information content and utility of these signals changes as the imaging rate changes. In the next section, we describe these signals as well as a few signals derived from the cantilever and used in the TM-AFM (detection-based) approach. We then study these signals and their utility at different tip speeds through experiments with a linear grating.

## 2. OVERVIEW OF THE ACCESSIBLE SIGNALS IN THE Z-LOOP OF AFM

The allowable imaging rate of an AFM is typically well below the lowest bandwidth of the mechanical components of the system, including the cantilever and the piezoelectric actuator in the vertical ( $z$ -) direction. A block diagram of a typical  $z$ -loop is given in Fig. 1, together with the derived signals of the TM-AFM approach. A typical commercial AFM produces images primarily from the controller output and the amplitude and phase signals. Details on this process can be found in (Abramovitch et al., 2007).

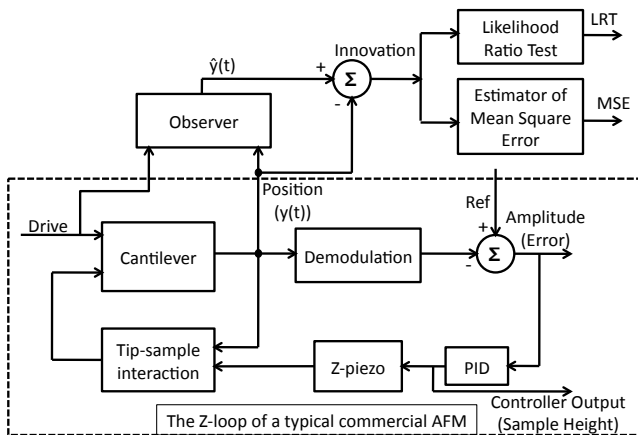


Fig. 1. Illustration of the structure of a typical  $z$ -loop in an AFM. The dashed box contains the control loop of a typical commercial AFM while outside of the box are signals generated from the cantilever motion.

At speeds beyond the bandwidth of the closed-loop system, the height value becomes corrupted and cannot be relied upon to produce a good image. Nevertheless, the signals in the system still carry valuable information. Motivated by this, the TM-AFM technique uses an observer to estimate the state of the cantilever, generating an innovation signal that can be further processed to detect impacts (caused by sample edges). The innovation sequence, however, contains more information than just the onset of a transient and in this paper we also consider the mean-squared error (MSE) of the innovations, originally described in (Tathagata De and Salapaka, 2006).

In the remainder of this section, we describe in more detail the signals we are interested in.

### 2.1 Height

In amplitude-modulated tapping mode, the change in the amplitude of the oscillation of the cantilever while scanning is controlled to a set value by adjusting the vertical position of the  $z$ -piezo. As illustrated in Fig. 1, this motion is typically commanded by a PID or similar simple controller. For accurate imaging, the time interval between the measurements in two pixels should be sufficient for all the blocks along the loop to recover to their steady states. In this scenario, the output of the PID controller is representative of the sample height and is therefore taken as the height image. As the tip speed is increased, the height signal begins to be corrupted by the dynamics of the piezo actuator, leading to controller and dynamic artifacts in the height signal. Note that this can occur even at speeds well below the closed-loop bandwidth. At even higher tip speeds, the controller cannot respond to the disturbance caused by the sample and the height signal loses all information. As a result, high quality imaging always incurs a large cost in terms of imaging time.

### 2.2 Amplitude

The amplitude signal is the error signal in the control loop. Since the cantilever is oscillating at a frequency close to its resonance, the magnitude of the motion is sensitive to the external disturbance of the sample. As the tip scans over the sample surface, the profile change of the sample drives a change in the magnitude of the cantilever vibration. When scanning within the allowable imaging rate, the controller regulates the error signal back to zero. As a result, the amplitude signal in essence acts as an edge detector and can be used to enhance the contrast in an image along the edges of the sample. It can often also provide a clearer image of small elements attached to a large object. As an edge detector, it has also been used in the LRS scheme to determine when the tip crosses on and off of a string-like sample.

As the tip speed is increased enough so that the controller can no longer regulate the error signal, the amplitude begins to reflect the topology of the sample. As noted in Fig. 1, the error signal is derived from the cantilever motion by demodulating the drive signal generating the oscillation. At even faster tip speeds, then, the rates become comparable to or faster than the rate of demodulation and the amplitude signal becomes corrupted with the dynamics of the demodulator. To avoid those dynamics, one can step back to the cantilever signal and consider other derived signals; this is the idea behind the transient signal method.

### 2.3 Innovation process

The cantilever signal has the highest bandwidth of any of the signals in the loop with typical resonant frequencies from the tens to the hundreds of kHz. By taking advantage of very small cantilevers, these frequencies can even be pushed into the MHz range (Schaeffer et al., 1997). The fundamental idea of the transient method is to use a model-based observer to estimate the state of the cantilever and to view the nonlinear tip-sample interaction as abrupt jumps acting on the system. Cantilever dynamics

can in general be well approximated by a second-order system (Stark et al., 2004) and generally one can write

$$x(k+1) = \Phi(k+1, k)x(k) + w(k) + \delta_{\theta, k+1}\vartheta, \quad (1a)$$

$$y(k+1) = H(k+1)x(k+1) + \nu(k), \quad (1b)$$

where  $\Phi(k+1, k)$  is the transition matrix,  $w(k)$  and  $\nu(k)$  are thermal and measurement noise given by independent, zero mean, white Gaussian random processes with  $E[w(k)w^T(k)] = Q(k)$  and  $E[\nu(k)\nu^T(k)] = R(k)$ ,  $\delta_{\theta, k+1}$  is a delta function input, and  $\vartheta$  is the magnitude of the (possible) impulsive input.

An observer (often a Kalman observer) can be designed to estimate the state of the system,

$$\hat{x}(k+1|k) = \Phi(k+1, k)\hat{x}(k|k), \quad (2a)$$

$$\hat{x}(k+1|k+1) = \hat{x}(k+1|k) + K(k)\gamma(k), \quad (2b)$$

$$\hat{y}(k+1) = H(k+1)\hat{x}(k+1|k+1) \quad (2c)$$

where  $\gamma(k) = y(k) - \hat{y}(k)$  is the innovation process and  $K(k)$  is the observer gain. Note that typically a steady state value of the observer gain is used in the implementation to avoid the computational cost of calculating the dynamics of the gain.

While scanning over a flat surface, the observer closely follows the actual cantilever system, leading to an innovation signal that is a zero mean white Gaussian stochastic process. Whenever there is a change in the sample profile, the cantilever system encounters an abrupt input and the corresponding mismatch of the initial conditions between the system and the observer causes the innovation to lose its zero mean property until the observer recovers.

#### 2.4 Likelihood Ratio Test (LRT)

The decision as to whether the innovation signal is zero-mean or non-zero mean can be formulated in a standard binary hypothesis framework,

$$H_0 : \gamma(k) = \gamma_1(k), \quad (3a)$$

$$H_1 : \gamma(k) = G(k; \theta)\nu + \gamma_1(k), \quad (3b)$$

where  $\gamma_1(k)$  is a zero mean white Gaussian stochastic process (modeling the measurement residual in the absence of impulses) and  $G(k; \theta)$  is a function of a window of time with a value that depends on the parameters of the cantilever dynamics and the observer, the time an impulse is applied and the corresponding gain of that impulse. The decision between the hypotheses is made using a generalized likelihood ratio test. Details of the derivation of  $G(k; \theta)$  as well as the computation of the likelihood ratio can be found in (Willisky and Jones, 1976).

#### 2.5 Estimate of the mean square error

Under the assumption that the innovation process is white Gaussian noise, it can be completely described by its first and second order moments. The likelihood ratio signal is driven only by changes in the mean of the process but changes in the variance also contain information about the sample. This motivates the development a new estimator, namely the mean square error over a window size  $M$ , given by

$$\hat{\sigma}^2(k) = \sum_{i=k-M+1}^k \frac{\gamma^2(i)}{M}. \quad (4)$$

Selection of the window size depends on the speed of scanning and should be such that there is only a single impulsive input in each window.

#### 2.6 Discussion of the transient-based detection

The use of the observer highlights both the benefits and the limitations of some of these signals. Using the observer, innovation sequence, and likelihood ratio, edges in the sample can be detected rapidly, typically with a bandwidth a quarter of the resonant frequency of the cantilever used (Sahoo et al., 2005). Ignoring dynamics and challenges in the control of the scanning direction, the imaging rate can be roughly estimated by assuming that the bandwidth sets the lower limit on the measurement time of each pixel. Based on this, using a cantilever with a resonant frequency of 400 kHz can lead to scanning of a sample with a resolution of  $200 \times 200$  in approximately 0.4 seconds. If this approach is coupled with the LRS method for scanning biopolymers and other string like samples, then an additional order of magnitude improvement coming from the reduced scan size yields a frame rate on the order of 25 frames per second.

It should be noted, however, that the technique only reveals edges that increase in height. Due to the nature of the nonlinear tip-sample interaction, a step-down in the sample leads to a mild change in the force acting on the cantilever, falsifying the assumption of an impulsive input. Thus the transient method can accurately reveal only edges in one direction.

### 3. EXPERIMENTAL RESULTS

In this section we describe experimental results for all of the signals described in Sec. 2.3.

#### 3.1 Experimental setup

All experiments were performed on an Agilent 5500 equipped with a MAC III module and operated in its Acoustic AC (AAC) mode (a form of tapping mode). The manufacturer's specifications give the bandwidth of the open-loop piezoelectric actuators in all directions to be in the range of 5 kHz – 10 kHz, with closed-loop to be around 1 kHz. A sequence of scans with tip speeds of 4  $\mu\text{m/s}$ , 40  $\mu\text{m/s}$ , 400  $\mu\text{m/s}$  and 4000  $\mu\text{m/s}$  was performed. The first two speeds were slow enough to produce good quality images from the height signal, the third is comparable to the  $z$ -loop bandwidth of the instrument, while the last is far beyond this bandwidth. The last two are expected to produce very poor images from the standard signals (height and amplitude). All the scans were performed on a linear grating (TGZ01, MikroMash) with a feature height of 20 nm and a pitch width of 3.3  $\mu\text{m}$ .

The data acquisition and the implementation of the observer and the mean square error (see Sec. 2.3) were done using a compact Reconfigurable Input-Output (cRIO) system (cRIO 9076, National Instruments). This system includes an embedded 400 MHz real-time processor and an LX45 FPGA from the Xilinx Spartan-6 family. The cRIO was outfitted with a 1Ms/s high-speed analog-digital converter (ADC) (NI 9215, National Instruments)

Table 1.

Tip Speed ( $\mu\text{m/s}$ , Lines/s)	Scanning Range ( $\mu\text{m}$ )	Number of Pixels	Results Shown in
4, 0.2	10	512	Fig. 2
40, 1	20	512	Fig. 3
400, 8	20	512	Fig. 4
4000, 24	90	512	Fig. 5

for sampling the cantilever position, cantilever drive and the cantilever amplitude (deflection), a 100Ks/s ADC (NI 9223, National Instruments) for sampling the  $z$ -controller output for the height information of the sample, a 100Ks/s digital-to-analog converter (DAC) and a digital input and output (DIO) card for possible triggering applications. The software was written in LabView 12.0 (National Instruments).

Due to the complexity of calculation, the likelihood ratio was calculated offline.

### 3.2 Scanning results and discussion

The scanning parameters used are shown in Table. 1 and the corresponding signals from the scans are shown in Figs. 2-5. These figures illustrate that there is useful information in all the signals but that the best choice depends on the scanning speed and the application.

The images that best captured the topography of the sample are clearly those taken at 0.2 lines/s (Fig. 2) but at the cost of waiting 42 minutes to acquire the image. At this low speed, the PID control kept the error signal in good regulation, leading to quality images. At the same time, this good regulation kept the amplitude signal near zero, preventing it from being used to detect edges and thus for use in detection-based schemes such as LRS. The signals from the transient-based detector were also essentially devoid of information about the sample. This is because at this speed, encounters with the sample edges cannot be modeled as a delta function input.

When the tip speed was increased to 40  $\mu\text{m/s}$  (1 line/s), shown in Fig. 3, the controller performance was somewhat degraded. This image was acquired in 8 minutes but yielded a poorer topography image; the linear gratings were no longer straight and the height value was not uniform along the edge. At the same time, this faster speed yielded a clearer amplitude image than before as the overshoot at each edge was greater (see Fig. 3(c)). With these clear peaks, it becomes possible to use an algorithm such as the LRS to speed up the acquisition of images of string-like samples from eight minutes to just under one minute for equivalent resolution. This speed was still too slow, however, to model the tip encounters with the sample edges as delta functions and as a result neither the innovation signal nor the likelihood ratio contains useful information. Surprisingly, the MSE provided small but distinct peaks at the step-ups and step-downs of the grating.

In the third scan, the tip speed was increased so that the scanning rate was comparable to the bandwidth of the closed-loop system. This can be seen in Fig. 4(c) where the amplitude signal barely has time to return to steady state before the next edge occurs, implying that the time interval between edges is approximately the same as that

defined by the bandwidth of the closed-loop system. At this speed the height signal is no longer reliable and the topography shows nothing more than the edges in the sample. As seen in Fig. 4(d), the innovation sequence now has small spikes at the sample edges. These spikes are significantly amplified in the likelihood ratio signal. The MSE signal has clear positive and negative going spikes at each edge of the sample. The images took approximately one minute to acquire. If accurate topography were not a priority, the height and amplitude signals still reveal useful information. The LRS algorithm could also be applied to reduce the imaging time down to approximately six seconds, using either the amplitude or the likelihood ratio signals as a detector for the algorithm.

In the last scan, shown in Fig. 5, the upper limit of the tip speed of the instrument was used, yielding approximately 4000  $\mu\text{m/s}$ . In order to achieve this tip speed, the scanning range was set to 90  $\mu\text{m}$ . With this large scan area and high speed, issues such as tilt in the sample surface caused failure of the engagement of the tip for portions of each scan with only a small portion of the range having good engagement. The data shown represents only this region of good engagement. The speed was far beyond the timescale set by the bandwidth of the controller and thus the height signal (shown in Fig. 5(a)) became meaningless. Similarly, the amplitude signal could not be brought back to steady state between two edges. The decay rate of the innovation signal, however, is defined by the gain of the observer. As can be seen in Fig. 5(d), the innovations now have clear spikes at every positive going edge. These spikes are amplified by the likelihood ratio. Interestingly, the MSE signal contains a reasonable estimate of the features in the sample, though with irregular amplitudes.

## 4. SCANNING AT DIFFERENT ANGLES

It is possible that the direction at which the tip crosses the sample may have significant impact on the dynamics in the signals. It is not expected that this direction would be important at the slower scanning speeds where the controller can adequately respond to disturbances but at the higher rates, different angles may affect the amplitude or other derived signals. To investigate this, we repeated the scans at tip speeds of 400  $\mu\text{m/sec}$  and 4000  $\mu\text{m/sec}$  at scan angles of 30°, 45°, and 60°. Representative results are shown for the 45° scan in Fig 6.

These results indicate that while there may be a small effect on the derived signals, as seen by comparing Fig. 6(d) to the signals in Fig. 5(d), the angle does not significantly degrade their ability to represent the edges. It should be noted that changing the scan angle can also be interpreted as changing the local shape of the tip and thus these results provide some measure of robustness of the signals with respect to different tips.

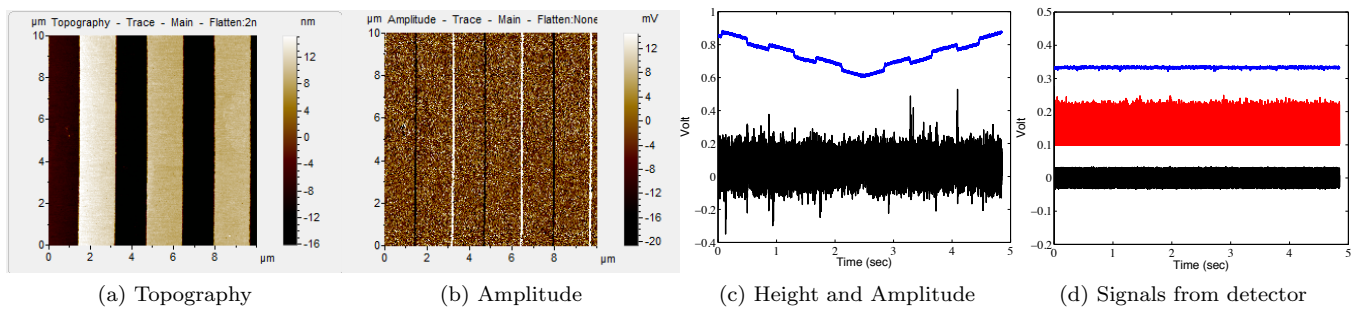


Fig. 2. Results from a line rate of 0.2 line/s with a scan range of 10  $\mu\text{m}$  (corresponding to a tip speed of 4  $\mu\text{m/s}$ ). (a) topography trace image; (b) amplitude trace image; (c) raw height (blue) and amplitude (black) signals from a portion of the scan; the sample tilt in the height signal is evident although the sample profile remains clear; (d) innovation signal (black), likelihood ratio (red), and MSE (blue). The innovation and likelihood ratio show no clear indication of the edges in the sample while the MSE has occasional negative spikes at those locations.

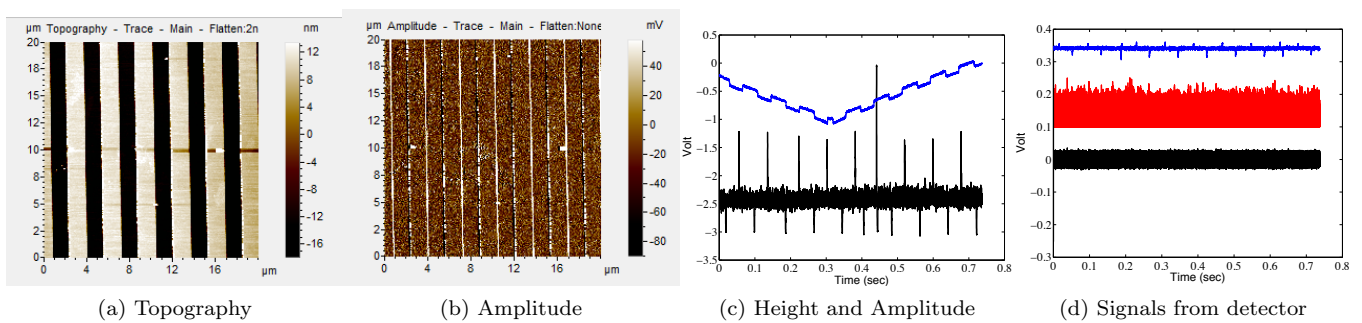


Fig. 3. Results from a line rate of 1 line/s with a scan range of 20  $\mu\text{m}$  (corresponding to a tip speed of 40  $\mu\text{m/s}$ ). (a) topography trace image; (b) amplitude trace imaging; (c) raw height (blue) and amplitude (black) signals from a portion of the scan. The sample tilt is evident in the height signal although the sample profile remains clear (d) innovation signal (black), likelihood ratio (red), and MSE (blue). As with the slower speed, the innovation and likelihood ratio signals still show no clear indication of the sample edges. The MSE, however, now has clear positive and negative spikes at the step-up and step-down edges of the sample.

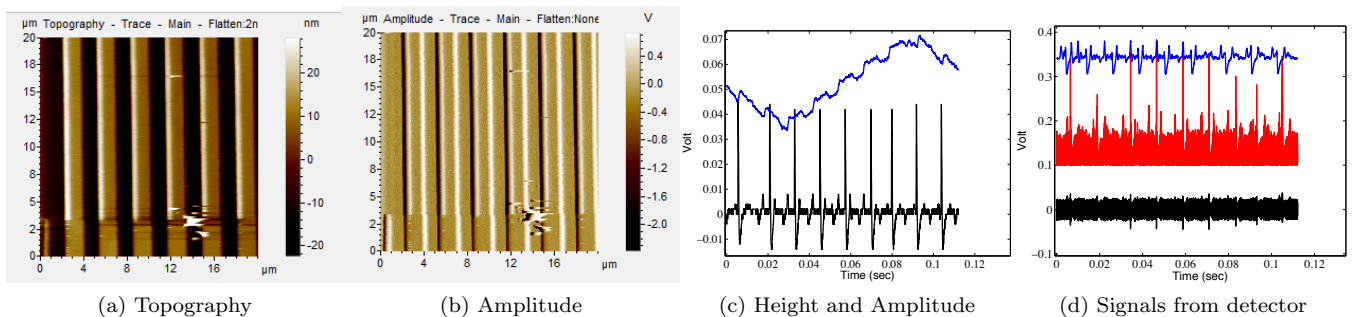


Fig. 4. Results from a line rate of 8 line/s with a scan range of 20  $\mu\text{m}$  (corresponding to a tip speed of 400  $\mu\text{m/s}$ ). (a) topography retrace image; (b) amplitude retrace image; (c) raw height (blue) and amplitude (black) signals from a portion of the scan. The sample tilt remains evident and the sample profile in the signal has become corrupted with the dynamics of the piezos and controllers. The amplitude signal has a stronger overshoot and longer transient than at slower speeds. (d) innovation signal (black), likelihood ratio (red), and MSE (blue). The innovation signal has some clear spikes at the sample edges which the likelihood ratio signal amplifies. The MSE signal still has clear positive and negative spikes at the step-up and step-down edges of the sample, though the width of those spikes is larger than at the slower tip speeds.

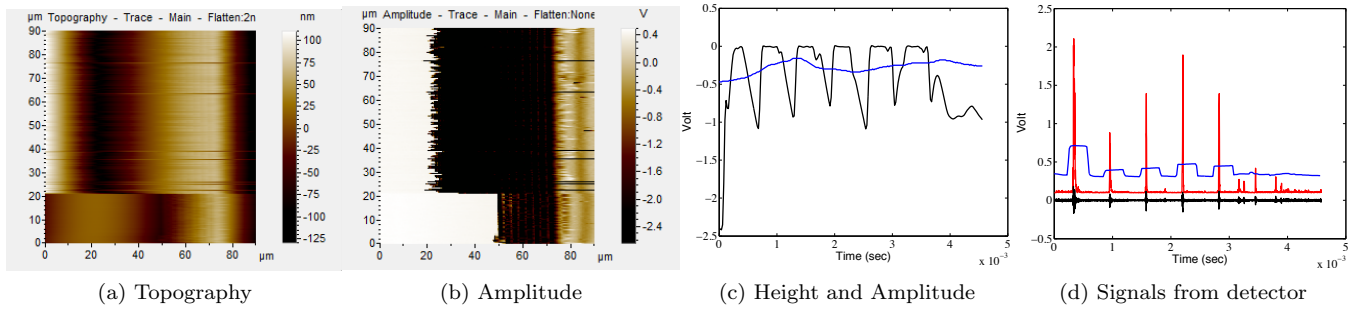


Fig. 5. Results from a line rate of 24 line/s with a scan range of 90  $\mu\text{m}$  (corresponding to a tip speed of 4000  $\mu\text{m/s}$ ); (a) topography retrace image; (b) amplitude retrace image. Both are clearly poor images (c) raw height (blue) and amplitude (black) signals. The height signal was completely corrupted and contained essentially no information about the sample topography. The amplitude signal was corrupted by the demodulation dynamics and similarly contained no information on the sample. (d) innovation signal (black), likelihood ratio (red), and MSE (blue). The innovation now shows clear peaks at the edges of the sample; these were strongly enhanced in the likelihood ratio signal. The MSE signal still has positive and negative edges at the corresponding sample edges and is now an estimate of the sample profile.

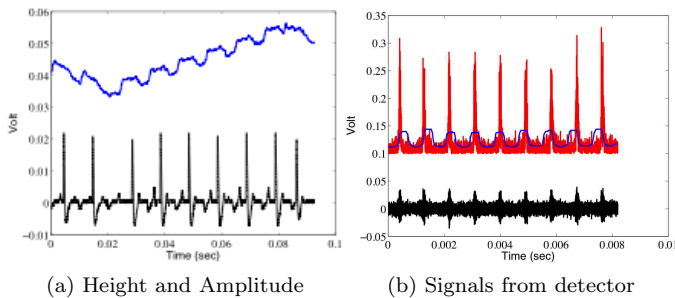


Fig. 6. Results from scanning at an angle of  $45^\circ$  relative to the calibration grating. (a) raw height (blue) and amplitude (black) signals at a scanning speed of 8 lines/s. Comparing (a) to the results in Fig. 4(c) illustrates little to no effect on the signal due to the scanning angle; (b) innovation signal (black), likelihood ratio (red), and MSE signal (blue) at a speed of 24 lines/s. Comparing to the results in Fig. 5(d) we see that at an angle of  $45^\circ$  the innovation and likelihood ratio show smaller peaks than at  $0^\circ$  but are still effective in representing the sample edges.

## 5. CONCLUSION

In this paper, we explored the information content of the signals in a typical commercial AFM using a linear grating. The signals explored were the height and amplitude that are for standard imaging as well as signals derived from a transient signal based detector. The results indicate that, as expected slow speeds are needed for the height signal to yield a good topography image. At these same slow speeds, however, the amplitude signal does not clearly denote sample edges. At slightly faster speeds, height begins to degrade but the amplitude signal becomes more useful in enhancing the edge contrast in the images. For techniques relying on transient effects for detection, including TM-AFM and the LRS algorithm, the tip speed must be sufficiently high to allow for accurate detection. For good imaging with the LRS algorithm, then, the amplitude signal is the most obvious choice for edge detection. The results also indicated that the tip can be

moved at speeds far beyond the controller bandwidth while maintaining good detection of the sample edges. This idea has been used effectively in the TM-AFM scheme and also illustrates that sample edges can be traversed very rapidly using the LRS algorithm.

We note that in the context of this paper, the timescale defining what is “slow” and what is “fast” is set by the bandwidth of the  $z$ -controller, though of course dynamics of the lateral scanning are also important to good imaging. Most approaches to high speed AFM rely in part on methods to increase this bandwidth. The results in this paper are applicable to those systems as well.

## REFERENCES

- Abramovitch, D.Y., Andersson, S.B., Pao, L.Y., and Schitter, G. (2007). A tutorial on the mechanisms, dynamics, and control of atomic force microscopes. 3488–3502.
- Binnig, G. and Quate, C.F. (1986). Atomic force microscope. *Physical Review Letters*, 56, 930–933.
- Braunsmann, C. and Schaffer, T.E. (2010). High-speed atomic force microscopy for large scan sizes using small cantilevers. *Nanotechnology*, 21, 225705.
- Chang, P., Huang, P., Maeng, J., and Andersson, S. (2011). Local raster scanning for high speed imaging of biopolymers in atomic force microscopy. *Review of Scientific Instruments*, 82, 063703 (7 pages).
- Huang, P. and Andersson, S.B. (2012). Fast detection based on semi-transient signals in afm. 3216–3221.
- Kenton, B.J., Fleming, A.J., and Leang, K.K. (2011). Compact ultra-fast vertical nanopositioner for improving scanning probe microscope scan speed. *Review of Scientific Instrument*, 82, 123703.
- Kodera, N., Yamamoto, D., Ishikawa, R., and Ando, T. (2010). Video imaging of walking myosin V by high-speed atomic force microscopy. *Nature*, 468, 72–76.
- Sahoo, D.R., Sebastian, A., and Salapaka, M.V. (2005). Harnessing the transient signals in atomic force microscopy. *International Journal Of Robust And Non-linear Control*, 805 – 820.
- Salapaka, S., De, T., and Sebastian, A. (2005). Sample-profile estimate for fast atomic force microscopy. *Applied*

- Physics Letters*, 87, 053112 (3 pages).
- Schaeffer, T.E., Viani, M., Walters, D.A., Drake, B., Runge, E.K., Cleveland, J.P., Wendman, M.A., and Hansma, P.K. (1997). Atomic force microscope for small cantilevers. *SPIE. Proceedings*, 3009, 48–52.
- Shan, Y. and Leang, K.K. (2012). Accounting for hysteresis in repetitive control design: Nanopositioning example. *Automactica*, 48, 1751–1758.
- Stark, R.W., Schitter, G., Stark, M., Guckenberger, R., and Stemmer, A. (2004). State-space model of freely vibrating and surface-coupled cantilever dynamics in atomic force microscopy. *Physical Review B*, 69, 085412.
- Tathagata De, Pranav Agarwal, D.R.S. and Salapaka, M.V. (2006). Real-time detection of probe loss in atomic force microscopy. *Applied Physics Letters*, 89, 133119.
- Viani, M.B., Pietrasanta, L.I., Thompson, J.B., Chand, A., Gebeshuber, I.C., Kindt, J.H., Richter, M., Hansma, H.G., and Hansma, P.K. (2000). Probing protein–protein interactions in real time. *Nature Structural Biology*, 7, 644–647.
- Willsky, A.S. and Jones, H.L. (1976). A generalized likelihood ratio approach to the detection and estimation of jumps in linear systems. *IEEE Transaction on Automatic Control*, Feb, 108–112.
- Wu, Y. and Zou, Q. (2007). Iterative control approach to compensate for both the hysteresis and the dynamics effects of piezo actuators. *IEEE Transactions on Control Systems Technology*, 15, 936–944.